JACS
JOURNAL OF THE AMERICAN CHEMICAL SOCIETY

Article

pubs.acs.org/JACS

Constructing Ultraporous Covalent Organic Frameworks in Seconds via an Organic Terracotta Process

Suvendu Karak,[†,‡] Sharath Kandambeth,[†,‡] Bishnu P. Biswal,[†,‡] Himadri Sekhar Sasmal,[†,‡] Sushil Kumar,[‡] Pradip Pachfule,[‡] and Rahul Banerjee*[,†,‡]

[†]Academy of Scientific and Innovative Research (AcSIR), New Delhi 110025, India

[‡]Physical/Materials Chemistry Division, CSIR-National Chemical Laboratory, Dr. Homi Bhabha Road, Pune 411008, India

Supporting Information

ABSTRACT: Research on covalent organic frameworks (COFs) has recently gathered significant momentum by the virtue of their predictive design, controllable porosity, and long-range ordering. However, the lack of solvent-free and easy-to-perform synthesis processes appears to be the bottleneck toward their greener fabrication, thereby limiting their possible potential applications. To alleviate such shortcomings, we demonstrate a simple route toward the rapid synthesis of highly crystalline and ultraporous COFs in seconds using a novel salt-mediated crystallization approach. A high degree of synthetic control in interlayer stacking and layer planarity renders an ordered network with a surface area as high as 3000 m^2 g^{-1}. Further, this approach has been extrapolated for the continuous synthesis of COFs by means of a twin screw extruder and *in situ* processes of COFs into different shapes mimicking the ancient terracotta process. Finally, the regular COF beads are shown to outperform the leading zeolites in water sorption performance, with notably facile regeneration ability and structural integrity.

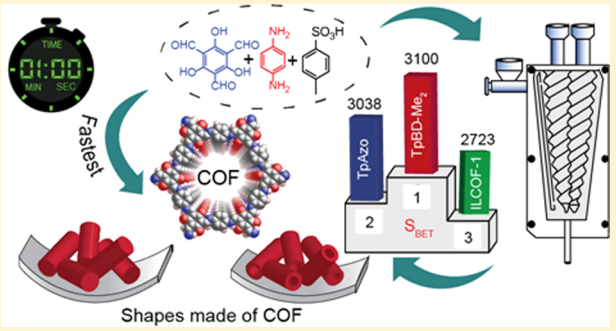

INTRODUCTION

Covalent organic frameworks (COFs)[1−6] have summoned substantial amount of attention in the past decade owing to their unique designing features as well as enormous potentials.[6−16] The conventional synthetic route to obtain such ordered covalent networks is the modular connection of a vast array of rigid and symmetrical building blocks through covalent bonds. In this regard, the process of solvothermal synthesis[17−19] has emerged as a forerunner leading to the invention of a significant number of highly crystalline COFs. Sometimes, but not limited to all the cases, tedious synthetic procedures and longer reaction times (72−90 h) create hurdles in the detailed explorations of the diverse potentials of COFs. Although mechanochemical,[20,21] ionothermal,[22] sonochemical,[23] microwave,[24] and microfluidic[25,26] syntheses routes have been used as alternatives, in most of these cases the final product results with moderate porosity and limited crystallinity. Thus, a simpler and solvent-free synthetic route is desirable for the generation of porous COFs, which would combine the merits of (i) the solvothermal process, high crystallinity; (ii) the mechanochemical process, low environmental impact; and (iii) the microwave process, fast reaction rate.

Herein, we present an eloquent methodology of exceptionally rapid synthesis of COFs which proceeds through a molecular organization approach. We have introduced a Bronsted acid, *p*-toluenesulfonic acid (PTSA−H_2O), as a molecular organizer, which induces the reversibility[27] and results in an ordered network[28] with higher crystallinity and ultrahigh porosity by minimizing the defects in the framework. We have synthesized 12 highly crystalline COFs with a surface area as high as 3109 m^2 g^{-1} in 60 s, which is highest among all the two-dimensional COFs reported. We have also explored the large-scale (∼10 g/h) synthesis of COFs with high surface area, good crystallinity, and high chemical stability using a twin screw extruder (TSE). Further, this method has been successfully implemented for the *in situ* processing of COFs into various shapes (hollow tubes, cylinders, beads, and membranes) and sculptures, mimicking the ancient terracotta process, which consists of three essential steps: clay preparation, mold making, and baking. The potential shapes (beads and cylinders) possess high porosity, crystallinity, and thermochemical stability comparable to those of their parent powdered forms. We further exploited the water adsorption capacity of the COFs in both powdered and shaped forms using static and dynamic water adsorption measurements.

RESULTS AND DISCUSSION

First, the *p*-toluenesulfonic acid (2.5 mmol) and 12 separate diamines were mixed thoroughly. 1,3,5-Triformylphloroglucinol (**Tp**) (0.3 mmol) was then added into the mixture, followed by the addition of ∼100 μL water. The resulting material was mixed well until it gets converted into dough, which was further heated at 170 °C for 60 s. The resulted deep reddish powder

Received: August 30, 2016
Published: January 20, 2017

DOI: 10.1021/jacs.6b08815
J. Am. Chem. Soc. 2017, 139, 1856−1862

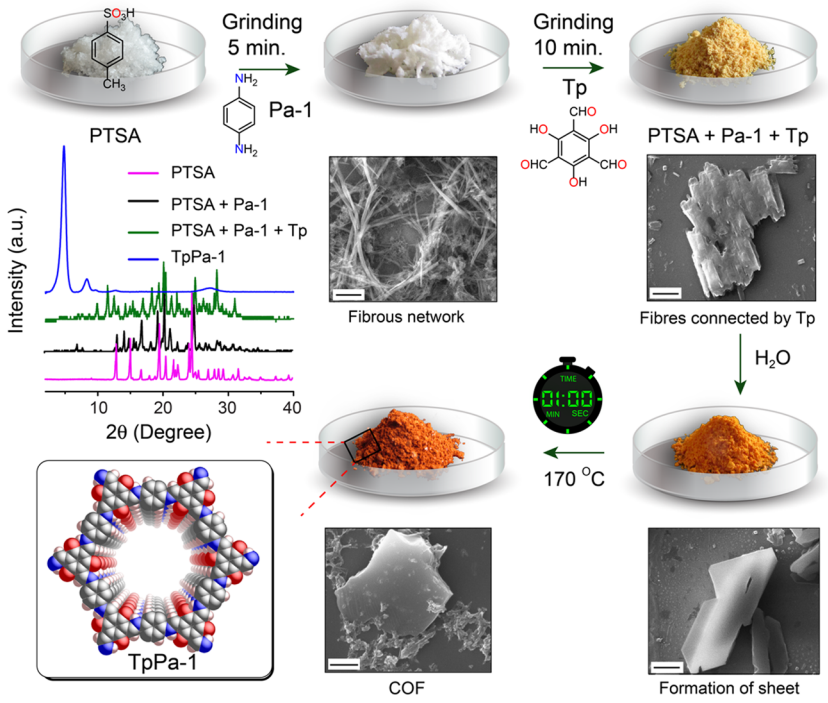

Figure 1. Synthesis of COFs via a molecular organization approach with sequential SEM and PXRDs of each individual crystallization steps.

was dipped into 500 mL of hot water for 5 min to isolate 12 highly crystalline porous COFs in powdered form with more than 90% isolated yield (Figure 1). It is important to note that, before heating, the soft dough could be molded into geometrical shapes and different sculptures without the use of additional binder, and then subjected for baking to obtain the COFs in desired shapes (*vide infra*).

The powder X-ray diffraction (PXRD) patterns of the **TpPa** series COFs (**TpPa-1**[6], **TpPa-2**[6], and **TpPa-NO$_2$**[29]) show a high intense first peak at ~5° (±0.2, 2θ), which could be attributed to the strong reflection from (100) planes (Figure 2). Similarly, a broad peak at higher 2θ value (~27.4° ±0.2) signifies the π–π stacking arising from (001) planes. On the other hand, **TpBD**,[20] **TpBD-Me$_2$**,[29] **TpBD-(NO$_2$)$_2$**,[29] **TpBD-(OMe)$_2$**,[29] **TpAzo** (**Tp-Azo**),[11] **TpAnq** (DAAQ-TFP),[15] **TpBpy**,[13] **TpTph** (UCBZ-5),[30] and **TpTta** (TRIPTA)[31] show the presence of the first and most intense peak at ~3.6° (2θ), corresponding to the reflection from the (100) plane (Figure 2). The isoreticulation in the **TpBD** series COFs and **TpTph** leads to the larger pore apertures, resulting in certain shifts (2θ ≈ 1.4°) of the peak positions from higher to lower 2θ values. The experimental PXRD patterns are in good agreement with the simulated AA eclipsed stacking models, which match well with the previous literature reports (Figure S1, Supporting Information (SI)). The relatively high intensy (100) peak reflects the high crystallinity of these as-synthesized COFs.

The Fourier transform infrared spectroscopy (FTIR) of the as-synthesized COFs match well to those reported previously. The strong peaks at ~1256 cm^{-1} (−C−N) and ~1574 cm^{-1} (−C=C) clearly reveal the formation of the β-ketoenamine-linked framework structures (Figure S2, SI). These observations were further corroborated by the complementary solid-state ^{13}C NMR spectra, which clearly reveal a characteristic peak of the carbonyl carbon (C=O) at ~180–184 ppm (Figure S3a, SI). The scanning electron microscopy (SEM) images revealed the sheet-like morphology with 10–30 μm lateral dimensions for all the as-synthesized COFs in contrast to the previously reported 50–100 nm sized flower-like morphology obtained during the solvothermal synthesis (Figure S4, SI).[6] The high degrees of synthetic control, particularly over interlayer stacking and layer planarity, rendered an ordered network with large domain size. Transmission electron microscopy (TEM) was further used to explore the internal morphology of COFs, which confirms the layered morphology of these materials (Figure S5, SI). We assume that the sheet-like structures can be formed as a result of π–π stacking of different layers. The thermogravimetric analysis (TGA) of COFs in N_2 atmosphere showed thermal stabilities up to 300 °C, indicating the high thermal stability of these materials (Figure S3b, SI).

The architectural stability and permanent porosity, the foremost attributes of these COFs, were determined by N_2 adsorption analysis at 77 K. Among all the COFs reported in this paper, **TpBD-Me$_2$** possesses the highest Brunauer–Emmett–Teller (BET) surface area of 3109 m^2 g^{-1}, followed by 3038 (**TpAzo**), 2336 (**TpBpy**), 1432 (**TpPa-1**), 1400 (**TpBD**), 1343 [**TpBD-(OMe)$_2$**], 1027 (**TpAnq**), 1020 (**TpTph**), 850 (**TpPa-NO$_2$**), 825 (**TpTta**), 769 [**TpBD-(NO$_2$)$_2$**], and 538 m^2 g^{-1} (**TpPa-2**) (Figure 2). It is noteworthy that in most of the cases, there is almost 2–3-fold increase in the BET surface area compared to their previously reported solvothermal counterparts (see Figure 5a).[6,11,13,15,20,29−31] The high surface area of the as-synthesized COFs can be attributed to the larger particle dimensions, ordered pore channels, and long-range periodicity, which was reflected in the pore size distributions (Figure S6, SI), calculated using N_2 adsorption isotherms and high intensity (100) peaks observed in PXRD patterns of the COFs.

Mechanism. In order to gain insight into the origin of the periodicity of the as-synthesized COFs, we have carried out crystallinity and morphological studies of the COF particles

DOI: 10.1021/jacs.6b08815
J. Am. Chem. Soc. 2017, 139, 1856–1862

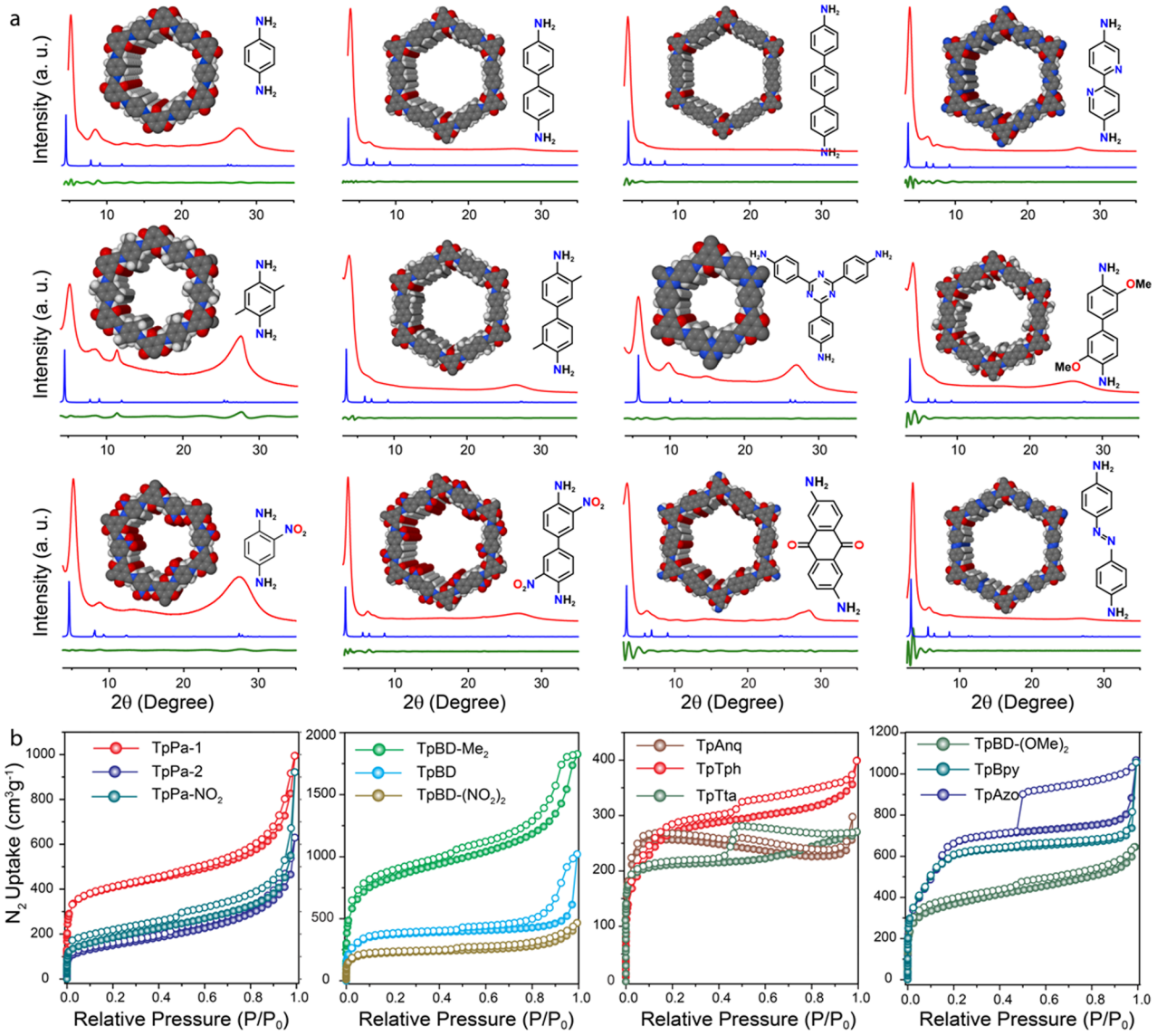

Figure 2. (a) Comparison of the experimental PXRD patterns (red) of COFs with the simulated eclipsed stacking model (blue) and their Pawley refinement difference (green). (b) Comparison of N_2 adsorption isotherms of all 12 COFs presented in this work.

during the course of the reaction using PXRD and SEM analyses (Figures S7c, S8, and S9, SI, Figure 3a). Traditionally, glacial acetic acid has been used to catalyze a variety of COF synthesis reactions, where the acidic proton tunes the reversibility of the reactions.[27,32,33] In the synthesis of the COFs reported herein, **PTSA** acts as a catalyst (Table S1 and Figures S10 and S11, SI)and further regulates the crystallization of the ordered framework structure connected entirely with covalent bonds. Acidic protons ($pK_a = -2.8$) on the sulfonic acid moieties of **PTSA** molecules easily protonate the primary N-atoms of the reacting amines and form **PTSA**-amine salts. These salt structures act as a template for the formation of the two-dimensional layers of COFs by taking the advantage of the H-bonded lamellar structures[28,34−36] of the **PTSA**-amine salts [**PTSA-Pa-1**, N−H···O; $D = 2.773(2)$ Å, $d = 1.886$ Å, $\theta = 164.1$; see Table S2, SI, for a full list of such H-bonding distances]. In each layer, the amine units are surrounded by **PTSA** molecules, and the distances between two adjacent protonated amine nitrogen range between 5 and 7 Å (N−N, D_N). The protonated amines can easily transfer the proton back to the **PTSA** during grinding with **Tp** (6.3 Å, O−O, D_O), and as a result of their similar dimensions (**PTSA** backbone and **Tp**), the incoming **Tp** can easily replace the existing **PTSA** unit (Figure S7c, SI) by breaking the weaker H-bonding interaction at the cost of the formation of a stable covalent bond (see Figure 3b and Figure S12, SI for a plausible mechanism). This leads to the further transformation of **PTSA**-amine fibers into sheets (Figure 3), which further gets stacked together by $\pi-\pi$ stacking interactions resulting into the formation of small COF crystallites. This mechanistic insight into improving the crystallinity and systematic control over the COF formation has also been investigated in the presence of various organic and inorganic acids. In this regard, the relationship between the amine−amine distance and the crystallinity of the resulting COFs was further investigated in a series of **PTSA**-amine crystals (6.54 Å for **Pa-1**, 5.33 Å for **Pa-2**, 5.48 Å for **Pa-NO$_2$**, 5.68 Å for **BD**) (Figures S13 and S14, SI). Thus, experimental data suggest that the N−N bond distance can be limited to a range of 5−7 Å. Similarly, other acids like phosphoric acid (**H_3PO_4**), trifluoromethyl carboxylic acid (**TFMC**) and 2-

DOI: 10.1021/jacs.6b08815
J. Am. Chem. Soc. 2017, 139, 1856−1862

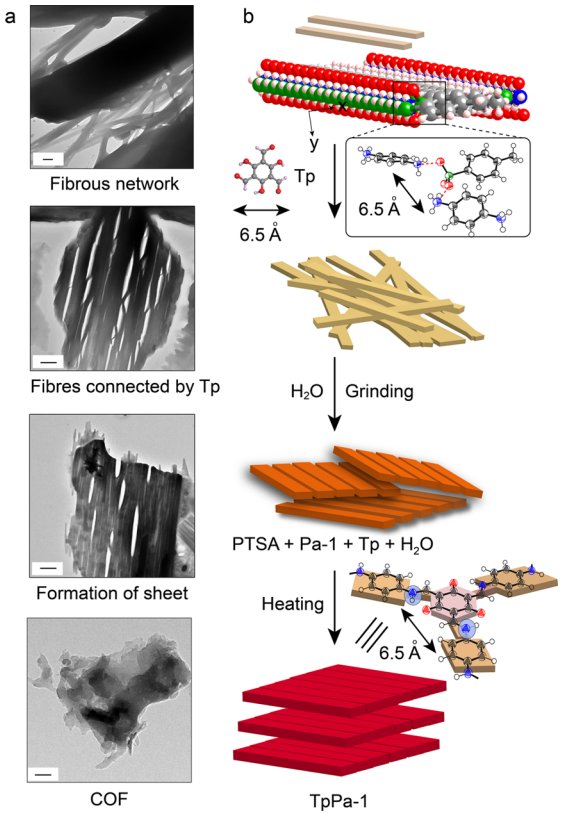

Figure 3. (a) TEM images at different stages of COF formation. (b) Model representation of the proposed mechanism of COF formation, considering **TpPa-1** as a model COF.

aminobenzenesulfonic acid (**ABSA**), phenol sulfonic acid (**PSA**), 4-nitrobenzenesulfonic acid (**NBSA**), and benzenesulfonic acid (**BSA**) have also been crystallized with **Pa-1**, and amine−amine distances among these salts are 6.75, 4.57, 4.95, 6.05, 3.68, and 5.49 Å, respectively (Figures S13 and S15, SI). When **H_3PO_4-Pa-1**, **TFMC-Pa-1**, **ABSA-Pa-1**, **PSA-Pa-1**, **NBSA-Pa-1**, and **BSA-Pa-1** salts have been reacted with **Tp** to synthesize **TpPa-1**, the resulting **TpPa-1** COF shows poor crystallinity and lower surface areas of 341, 75, 32, 648, 290, and 358 $m^2 g^{-1}$, respectively, compared to the value of 1432 $m^2 g^{-1}$ obtained by reacting **Tp** with **PTSA-Pa-1** (Table S4 and Figure S17, SI). From these examples, it is clear that the network formation is possible when the amine−amine distance ranges from 5 to 7 Å, as **Tp** can only replace **PTSA** within that range. In few cases, like **H_3PO_4-Pa-1**, **PSA-Pa-1**, and **BSA-Pa-1**, although the amine−amine distance fits the range of 5−7 Å, they still result in COFs with poor crystallinity, as either the acid−**Pa-1** salt does not form the lamellar structure or the hydrogen-bonding network is not directional for framework formation (Figure S15c−e, SI). The acid−amine reversible proton transfer also monitors the reversibility of the Schiff-base reaction by directing the backward reaction. Hence, the weaker hydrogen-bonding interaction as well as very strong hydrogen bonding affect the COF formation, resulting in less crystalline COFs with poor surface area. Thus, in the presence of phosphoric acid (**H_3PO_4**, $pK_a = 2.14$), trifluoromethanesulfonic acid [**TFMS**, $pK_a = -14.7$ (±2.0)], and acetic acid (**AcOH**, $pK_a = 4.7$), the as-synthesized COF **TpPa-1** results poor crystallinity with low surface area of 341, 188, and 4 $m^2 g^{-1}$, respectively (Figures S17 and S18, SI). We have also activated the as-synthesized COFs at 180 °C for 12 h to observe the effect of activation on the crystallinity and porosity of these materials. While activation improves the crystallinity and porosity of the materials, it is not found to be competitive with PTSA under similar experimental conditions (Table S5 and Figure S16, SI).

Beyond investigating the role of **PTSA**, the roles of other regulators, such as water and temperature, during the reaction pathway have also been analyzed. The addition of water in the **PTSA**−amine−**Tp** mixture inhibits the forward reaction of COF formation and maintains the breakage and formation of bonds, which systemically increases the crystallinity with the highly ordered molecular framework.[33,37] Heating the mixtures at different temperatures up to 60 s reveals that lower temperature (less than 100 °C) and shorter time duration (less than 40 s) provide poor crystallinity, which has been observed by time-dependent and variable-temperature PXRD patterns (Figure S7a,b SI). At a temperature as high as 170 °C, **PTSA**−amine−**Tp** mixture proceeds through a melting phase (excess **PTSA** melts down) that helps the sheets to reorganize (if time provided) into properly stacked form with highly crystalline[38] and ordered network structures.[39]

Large-Scale Processing. Solvent-free scalability is a crucial and highly demanding aspect of a sustainable chemical process. Although extruder is widely being used for polymer blending,[40,41] more recently, the application has further been extended for the synthesis of co-crystals[42] and MOFs.[43] Since the reversible covalent bond formation involves higher energy compared to the weaker supramolecular interactions and the residence times for the reactants in TSE are often only a few minutes or even seconds, the applications of the extrusion for COF synthesis is questionable.[43] Against this backdrop, we availed the opportunity of synthesizing COF in a TSE in the presence of **PTSA** with sequential addition of the amine, **PTSA**, and **Tp** followed by water. After continuing the extrusion for 5−10 min, the obtained mixture was left for heating at 170 °C for around 60 s (Figure 4). The resulting powder was washed several times with water, followed by drying in open air or in an oven preheated at 60 °C. PXRD and BET surface area measurements of the powder confirmed the formation of highly crystalline and porous COF materials (Figure S19, SI). It is also well observed that these COFs can be synthesized in high throughput rates of several kg h^{-1} by using large-scale equipment under a solvent-free continuous synthesis process.

COF Processability via Organic Terracotta Process. Processing the crystalline material into a desired geometric shape without any binder or plasticizer is subject to several limitations. Intricate problems like insolubility, chemical stability, scalability, and grain boundaries in conventionally synthesized discrete crystalline powders can cause difficulties in forming particular shapes. Additionally, the introduction of different plasticizers into the powder complicates the subsequent sintering process and contaminates the sintered material with undesired impurities. Therefore, an advanced synthetic route is highly desired to circumvent the aforementioned hurdles toward the development of porous COFs ofdifferent shapes for various applications. After mixing the **PTSA**, **Pa-1**, and **Tp**, the resulted dough (mentioned above) was processed into different shapes of cylinder, hollow tube, bead, membrane, and sculptures, which were further subjected for baking at 60−120 °C in a programmable oven for 12−24 h (Figure 4 and Figure S20a, SI). The slow heating helps the formation of COF shapes having a smooth surface with no cracks (Figures S21 and S22, SI). This process could be best

DOI: 10.1021/jacs.6b08815
J. Am. Chem. Soc. 2017, 139, 1856−1862

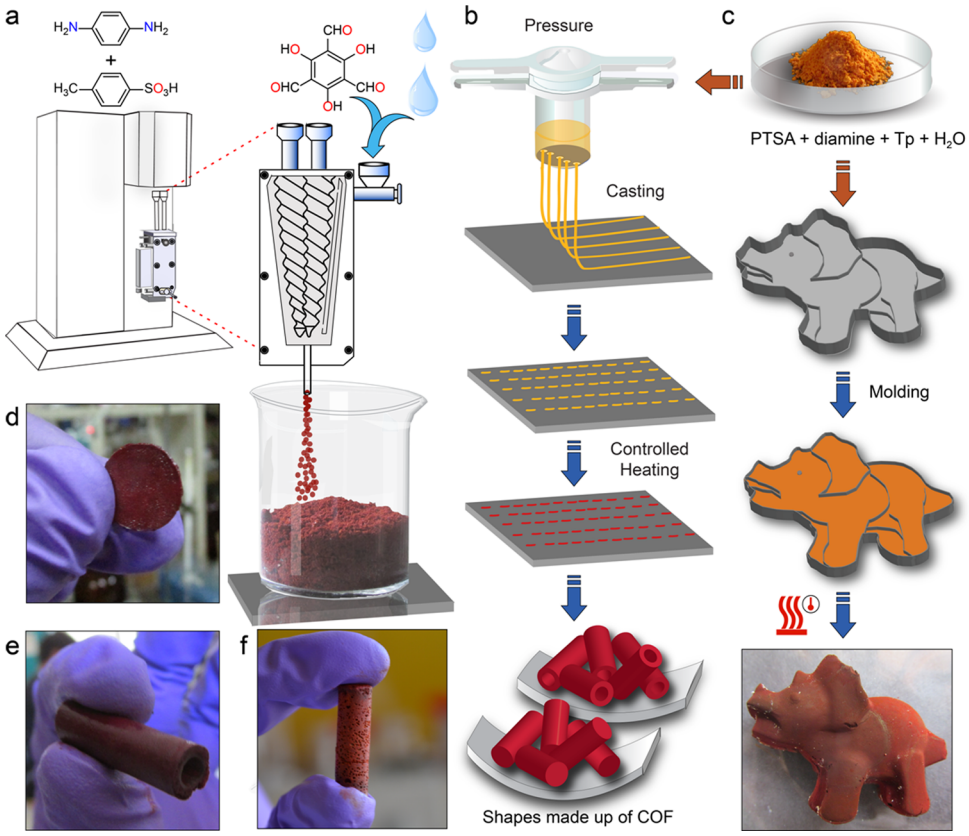

Figure 4. (a) COF synthesis by extrusion. (b) Schematic representation of COF-bead fabrication using the terracotta technique. (c) Schematic representation of COF processing into sculpture via the organic terracotta process. (d–f) Digital photographs of COF membrane, hollow tube, and cylinder, respectively.

compared with the ancient "terracotta process". Baking in the terracotta process involves chemical changes of the clay materials resulting from the removal of lattice water and quartz inversion, where the more random α-form changes to a more orderly β-quartz, resulting in a highly porous material. Similarly, in the present case, the byproduct water formed during the COF synthesis gets evaporated from the system during heating and finally gives rise to the porous ordered framework structure. We have fully characterized the derived shapes using standard methods such as PXRD, where we have confirmed that the shapes are composed of pure COF materials, devoid of any impurities (Figure S20b, SI). We have also performed the N_2 adsorption experiment on COF-beads, which shows the comparable BET surface area (1201 m^2 g^{-1}, **TpPa-1**) to that of their respective powdered form (1432 m^2 g^{-1}, **TpPa-1**) (Figure S20c, SI). The SEM images of the COF-shapes suggest that the shapes are basically constructed from the self-organization of sheets or platelet-like polymer crystallites (Figure S20e–h, SI). These regular shapes were next tested for stability for an extended period of time (7 days) in aqueous, acidic, and basic mediums as well as in different organic solvents such as *N,N*-dimethylformamide, acetonitrile, acetone, chloroform, hexane, and tetrahydrofuran. The shapes largely retained their inherent properties like crystallinity and porosity, keeping the structural aspects intact (Figure S23, SI).

Dehumidification Performance. Water adsorption in a porous material is inherently related to its framework porosity, condensation pressure of water in the pores, surface polarity, recyclability, and aqueous stability.[44] Although a step toward water adsorbing COFs has already been taken,[45,46] the major downside of these COFs, however, is their limited use in the powdered form. In this regard, we have considered that these COF shapes with high surface area, crystallinity, and hydrolytic stability will open up the ongoing development of COFs for dehumidification applications. The static water adsorption measurements of COFs performed at 298 K displayed sigmoidal-shaped type V isotherms, suggesting weak hydrophilic nature, but eventually adsorbing significantly high amount of water (Figure S20d, SI). Water adsorption capacity of 649 cm^3 g^{-1} (~52 wt%), 608 cm^3 g^{-1} (~49 wt%), 974 cm^3 g^{-1} (~78 wt%), and 756 cm^3 g^{-1} (~61 wt%) has been observed for **TpPa-1**, **TpAzo**, **TpBpy**, and **TpBD**, respectively; which may be attributed to the capillary condensation at $P/P_0 > 0.5$ (Figure 5c). These COFs outperform the currently used commercial water adsorbents such as Basolite A100 (20 wt%), zeolite NaX (33.6 wt%), zeolite 13X (33.3 wt%), silicoaluminophosphate SAPO-34 (33 wt%), and silica gel (32.7 wt%).[47] They also exhibit comparable water uptake with the recently reported MOFs such as MOF-808 (59 wt%), MOF-841 (51.4 wt%), Co-MOF-74 (50.6 wt%), and DUT-67 (50.2 wt%)[44] (Figure 5b). Additionally, the increased stability and recyclability of the COFs compared to those of the MOFs are expected to maximize the delivery of water and improve the COF utility under realistic process conditions. To evaluate these factors, we have collected the water adsorption isotherm up to four cycles repeatedly for **TpPa-1** and **TpBD** COFs processed in a cylindrical shape and compared with the first cycle (Figure S24a, SI), which show almost similar water adsorption. The surface area, FTIR, and PXRD patterns of these COFs were re-examined after the fourth cycle of water

DOI: 10.1021/jacs.6b08815
J. Am. Chem. Soc. 2017, 139, 1856–1862

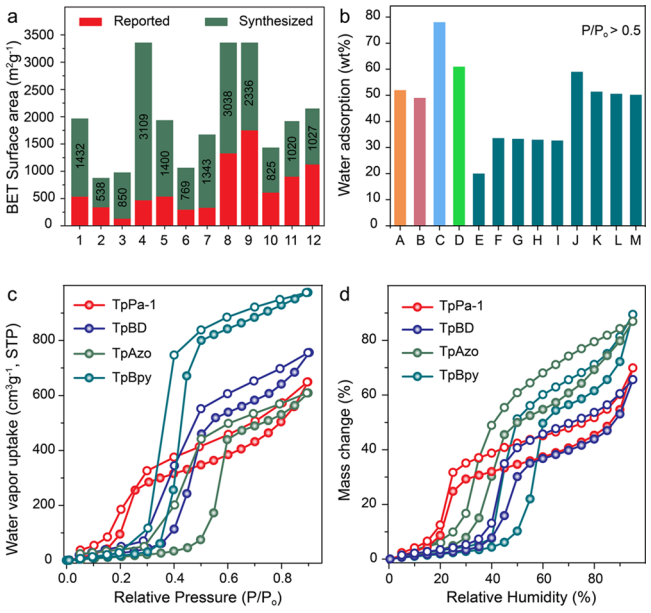

Figure 5. (a) BET surface area comparisons of the COFs [**TpPa-1** (1), **TpPa-2** (2), **TpPa-NO$_2$** (3), **TpBD-Me$_2$** (4), **TpBD** (5), **TpBD-(NO$_2$)$_2$** (6), **TpBD-(OMe)$_2$** (7), **TpAzo** (8), **TpBpy** (9), **TpTta** (10), **TpTph** (11), and **TpAnq** (12)] with their previous reports. (b) Water adsorption comparison of **TpPa-1** (A), **TpAzo** (B), **TpBpy** (C), and **TpBD** (D) with Basolite A100 (E), zeolite NaX (F), zeolite 13X (G), silicoaluminophosphate SAPO-34 (H), silica gel (I), MOF-808 (J), MOF-841 (K), Co-MOF-74 (L), and DUT-67 (M). (c) Static vapor sorption isotherm of **TpPa-1**, **TpAzo**, **TpBpy**, and **TpBD**. (d) Dynamic vapor sorption of **TpPa-1**, **TpAzo**, **TpBpy**, and **TpBD**.

adsorption, which shows insignificant changes, confirming the stability of COFs (Figure S24b,d, SI). We have further performed the dynamic vapor sorption at 45 °C. **TpPa-1** shows high water uptake at a relative humidity of less than 50%. A sharp increase in water uptake for **TpBD**, **TpAzo**, and **TpBpy** has been observed, when relative humidity reaches above 50% (Figure 5d). The high dynamic adsorption isotherm with respect to both relative pressure (869, 816, 1131, and 1081 $cm^3\ g^{-1}$ for **TpPa-1**, **TpBD**, **TpAzo**, and **TpBpy**, respectively) and humidity clearly suits them in continental and subcontinental conditions for potential dehumidification (Figure 5d and Figure S25, SI). A cost analysis indicates that **TpPa-1** costs around $752/100 g, assuming further optimizations in raw materials, along with COF formation for bulk-scale processing (Table S6, SI). Thus, practical estimated cost, superior performance, and facile regeneration keep COFs, in many respects, a step ahead of other solid desiccants used as dehumidifiers.

CONCLUSION

In summary, our findings overcome the long-term synthetic hurdles of COF synthesis and material processing by following a facile molecular organization method. Introduction of the organizer, *p*-toluenesulfonic acid, during the synthesis results in the formation of highly crystalline porous COFs in 60 s. A synthetic photocopy of the terracotta process enables us to process the COFs in different shapes with high crystallinity and ultrahigh porosity. Along with their rich reversible water adsorption, the synthetic easiness, scalability, and low cost will make these robust materials excellent candidates as dehumidifiers. Though we have correlated our synthetic understandings with crystallography, still there is much opportunity at the molecular level to be explored, and that will surely promote COFs a step forward as next-generation materials.

ASSOCIATED CONTENT

Supporting Information

The Supporting Information is available free of charge on the ACS Publications website at DOI: 10.1021/jacs.6b08815.

Synthesis, crystallographic, and characterization details (PDF)

X-ray crystallographic data for COFs (CIF)

AUTHOR INFORMATION

Corresponding Author

*r.banerjee@ncl.res.in

ORCID

Rahul Banerjee: 0000-0002-3547-4746

Notes

The authors declare no competing financial interest.

ACKNOWLEDGMENTS

S. Karak acknowledges University Grants Commission, Government of India, for a Junior Research Fellowship. R.B. acknowledges CSIR (CSC0122 and CSC0102), DST (SB/S1/IC-32/2013), DST Indo-Singapore Project (INT/SIN/P-05), and DST Nanomission Project (SR/NM/NS-1179/2012G) for funding. We acknowledge Dr. T. G. Ajithkumar for providing NMR, Dr. H. V. Pol for the extruder, and Dr. G. Kumaraswamy for use of the PXRD facility.

REFERENCES

(1) Côté, A. P.; Benin, A. I.; Ockwig, N. W.; Matzger, A. J.; O'Keeffe, M.; Yaghi, O. M. *Science* **2005**, *310*, 1166.

(2) Côte, A. P.; El-Kaderi, H. M.; Furukawa, H.; Hunt, J. R.; Yaghi, O. M. *J. Am. Chem. Soc.* **2007**, *129*, 12914.

(3) El-Kaderi, H. M.; Hunt, J. R.; Mendoza-Cortés, J. L.; Côté, A. P.; Taylor, R. E.; O'Keeffe, M.; Yaghi, O. M. *Science* **2007**, *316*, 268.

(4) Spitler, E. L.; Dichtel, W. R. *Nat. Chem.* **2010**, *2*, 672.

(5) Fang, Q.; Zhuang, Z.; Gu, S.; Kaspar, R. B.; Zheng, J.; Wang, J.; Yan, Y. *Nat. Commun.* **2014**, *5*, 4503.

(6) Kandambeth, S.; Mallick, A.; Lukose, B.; Mane, M. V.; Heine, T.; Banerjee, R. *J. Am. Chem. Soc.* **2012**, *134*, 19524.

(7) Furukawa, H.; Yaghi, O. M. *J. Am. Chem. Soc.* **2009**, *131*, 8875.

(8) Doonan, C. J.; Tranchemontagne, D. J.; Glover, T. G.; Hunt, J. H.; Yaghi, O. M. *Nat. Chem.* **2010**, *2*, 235.

(9) Oh, H.; Kalidindi, S. B.; Um, Y.; Bureekaew, S.; Schmid, R.; Fischer, R. A.; Hirscher, M. *Angew. Chem., Int. Ed.* **2013**, *52*, 13219.

(10) Ma, H.; Ren, H.; Meng, S.; Yan, Z.; Zhao, H.; Sun, F.; Zhu, G. *Chem. Commun.* **2013**, *49*, 9773.

(11) Chandra, S.; Kundu, T.; Kandambeth, S.; BabaRao, R.; Marathe, Y.; Kunjir, S. M.; Banerjee, R. *J. Am. Chem. Soc.* **2014**, *136*, 6570.

(12) Kandambeth, S.; Venkatesh, V.; Shinde, D. B.; Kumari, S.; Halder, A.; Verma, S.; Banerjee, R. *Nat. Commun.* **2015**, *6*, 6786.

(13) Shinde, D. B.; Aiyappa, H. B.; Bhadra, M.; Biswal, B. P.; Wadge, P.; Kandambeth, S.; Garai, B.; Kundu, T.; Kurungot, S.; Banerjee, R. *J. Mater. Chem. A* **2016**, *4*, 2682.

(14) Lohse, M. S.; Stassin, T.; Naudin, G.; Wuttke, S.; Ameloot, R.; De Vos, D.; Medina, D. D.; Bein, T. *Chem. Mater.* **2016**, *28*, 626.

(15) DeBlase, C. R.; Silberstein, K. E.; Truong, T.-T.; Abruña, H. D.; Dichtel, W. R. *J. Am. Chem. Soc.* **2013**, *135*, 16821.

(16) Xu, H.; Gao, J.; Jiang, D. *Nat. Chem.* **2015**, *7*, 905.

(17) Feng, X.; Ding, X.; Jiang, D. *Chem. Soc. Rev.* **2012**, *41*, 6010.

(18) Ding, S.-Y.; Wang, W. *Chem. Soc. Rev.* **2013**, *42*, 548.

DOI: 10.1021/jacs.6b08815
J. Am. Chem. Soc. 2017, 139, 1856−1862

(19) Waller, P. J.; Gandara, F.; Yaghi, O. M. *Acc. Chem. Res.* **2015**, *48*, 3053.
(20) Biswal, B. P.; Chandra, S.; Kandambeth, S.; Lukose, B.; Heine, T.; Banerjee, R. *J. Am. Chem. Soc.* **2013**, *135*, 5328.
(21) Das, G.; Shinde, D. B.; Kandambeth, S.; Biswal, B. P.; Banerjee, R. *Chem. Commun.* **2014**, *50*, 12615.
(22) Kuhn, P.; Antonietti, M.; Thomas, A. *Angew. Chem., Int. Ed.* **2008**, *47*, 3450.
(23) Yang, S.-T.; Kim, J.; Cho, H.-Y.; Kim, S.; Ahn, W.-S. *RSC Adv.* **2012**, *2*, 10179.
(24) Dogru, M.; Sonnauer, A.; Zimdars, S.; Doblinger, M.; Knochel, P.; Bein, T. *CrystEngComm* **2013**, *15*, 1500.
(25) Rodríguez-San-Miguel, D.; Abrishamkar, A.; Navarro, J. A. R.; Rodriguez-Trujillo, R.; Amabilino, D. B.; Mas-Ballesté, R.; Zamora, F.; Puigmartí-Luis, J. *Chem. Commun.* **2016**, *52*, 9212.
(26) Peng, Y.; Wong, W. K.; Hu, Z.; Cheng, Y.; Yuan, D.; Khan, S. A.; Zhao, D. *Chem. Mater.* **2016**, *28*, 5095.
(27) Mal, P.; Schultz, D.; Beyeh, K.; Rissanen, K.; Nitschke, J. R. *Angew. Chem., Int. Ed.* **2008**, *47*, 8297.
(28) Junggeburth, S. C.; Diehl, L.; Werner, S.; Duppel, V.; Sigle, W.; Lotsch, B. V. *J. Am. Chem. Soc.* **2013**, *135*, 6157.
(29) Chandra, S.; Kandambeth, S.; Biswal, B. P.; Lukose, B.; Kunjir, S. M.; Chaudhary, M.; Babarao, R.; Heine, T.; Banerjee, R. *J. Am. Chem. Soc.* **2013**, *135*, 17853.
(30) Zhu, Y.; Zhang, W. *Chem. Sci.* **2014**, *5*, 4957.
(31) Gomes, R.; Bhaumik, A. *RSC Adv.* **2016**, *6*, 28047.
(32) Tanoue, R.; Higuchi, R.; Enoki, N.; Miyasato, Y.; Uemura, S.; Kimizuka, N.; Stieg, A. Z.; Gimzewski, J. K.; Kunitake, M. *ACS Nano* **2011**, *5*, 3923.
(33) Belowich, M. E.; Stoddart, J. F. *Chem. Soc. Rev.* **2012**, *41*, 2003.
(34) Xu, C.; Zeng, Y.; Rui, X.; Xiao, N.; Zhu, J.; Zhang, W.; Chen, J.; Liu, W.; Tan, H.; Hng, H. H.; Yan, Q. *ACS Nano* **2012**, *6*, 4713.
(35) Zaworotko, M. J. *Chem. Commun.* **2001**, 1.
(36) Russell, V. A.; Evans, C. C.; Li, W.; Ward, M. D. *Science* **1997**, *276*, 575.
(37) Guan, C.-Z.; Wang, D.; Wan, L.-J. *Chem. Commun.* **2012**, *48*, 2943.
(38) Liu, X.-H.; Guan, C.-Z.; Ding, S.-Y.; Wang, W.; Yan, H.-J.; Wang, D.; Wan, L.-J. *J. Am. Chem. Soc.* **2013**, *135*, 10470.
(39) Ruben, M.; Payer, D.; Landa, A.; Comisso, A.; Gattinoni, C.; Lin, N.; Collin, J.-P.; Sauvage, J.-P.; De Vita, A.; Kern, K. *J. Am. Chem. Soc.* **2006**, *128*, 15644.
(40) Cardinaud, R.; McNally, T. *Eur. Polym. J.* **2013**, *49*, 1287.
(41) Yu, L.; Dean, K.; Li, L. *Prog. Polym. Sci.* **2006**, *31*, 576.
(42) Dhumal, R. S.; Kelly, A. L.; York, P.; Coates, P. D.; Paradkar, A. *Pharm. Res.* **2010**, *27*, 2725.
(43) Crawford, D.; Casaban, J.; Haydon, R.; Giri, N.; McNally, T.; James, S. L. *Chem. Sci.* **2015**, *6*, 1645.
(44) Furukawa, H.; Gandara, F.; Zhang, Y.-B.; Jiang, J.; Queen, W. L.; Hudson, M. R.; Yaghi, O. M. *J. Am. Chem. Soc.* **2014**, *136*, 4369.
(45) Stegbauer, L.; Hahn, M. W.; Jentys, A.; Savasci, G.; Ochsenfeld, C.; Lercher, J. A.; Lotsch, B. V. *Chem. Mater.* **2015**, *27*, 7874.
(46) Biswal, B. P.; Kandambeth, S.; Chandra, S.; Shinde, D. B.; Bera, S.; Karak, S.; Garai, B.; Kharul, U. K.; Banerjee, R. *J. Mater. Chem. A* **2015**, *3*, 23664.
(47) Seo, Y.-K.; Yoon, J. W.; Lee, J. S.; Hwang, Y. K.; Jun, C.-H.; Chang, J.-S.; Wuttke, S.; Bazin, P.; Vimont, A.; Daturi, M.; Bourrelly, S.; Llewellyn, P. L.; Horcajada, P.; Serre, C.; Férey, G. *Adv. Mater.* **2012**, *24*, 806.

DOI: 10.1021/jacs.6b08815
J. Am. Chem. Soc. 2017, 139, 1856−1862